BIOCHEMISTRY
including biophysical chemistry & molecular biology

Article

pubs.acs.org/biochemistry

Structural and Functional Insights into the Regulation of *Helicobacter pylori* Arginase Activity by an Evolutionary Nonconserved Motif

Abhishek Srivastava,[†,#] Shiv Kumar Meena,[†,#] Mashkoor Alam,[†] Shahid M. Nayeem,[‡] Shashank Deep,[‡] and Apurba Kumar Sau*[,†]

[†]National Institute of Immunology, Aruna Asaf Ali Marg, New Delhi 110 067, India

[‡]Department of Chemistry, Indian Institute of Technology, New Delhi 110 016, India

Supporting Information

ABSTRACT: Urea producing bimetallic arginases are essential for the synthesis of polyamine, DNA, and RNA. Despite conservation of the signature motifs in all arginases, a nonconserved [153]ESEEKAWQKLCSL[165] motif is found in the *Helicobacter pylori* enzyme, whose role is yet unknown. Using site-directed mutagenesis, kinetic assays, metal analyses, circular dichroism, heat-induced denaturation, molecular dynamics simulations and truncation studies, we report here the significance of this motif in catalytic function, metal retention, structural integrity, and stability of the protein. The enzyme did not exhibit detectable activity upon deletion of the motif as well as on individual mutation of Glu155 and Trp159 while Cys163Ala displayed significant decrease in the activity. Trp159Ala and Glu155Ala show severe loss of thermostability (14−17°) by a decrease in the α-helical structure. The role of Trp159 in stabilization of the structure with the surrounding aromatic residues is confirmed when Trp159Phe restored the structure and stability substantially compared to Trp159Ala. The simulation studies support the above results and show that the motif, which was previously solvent exposed, displays a loop-cum-small helix structure (Lys161−Cys163) and is located near the active-site through a novel Trp159−Asp126 interaction. This is consistent with the mutational analyses, where Trp159 and Asp126 are individually critical for retaining a bimetallic center and thereby for function. Furthermore, Cys163 of the helix is primarily important for dimerization, which is crucial for stimulation of the activity. Thus, these findings not only provide insights into the role of this motif but also offer a possibility to engineer it in human arginases for therapeutics against a number of carcinomas.

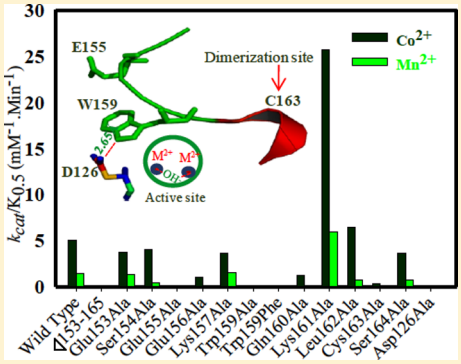

Helicobacter pylori (*H. pylori*) is a Gram-negative, microaerophilic bacterium, which infects half of the world population and is the causative agent of gastritis and peptic ulcers. It is associated with gastric cancer and labeled as class I carcinogen. Arginase (EC 3.5.3.1) is a binuclear Mn^{2+}-metalloenzyme. It is a member of ureohydrolase family and catalyzes the conversion of L-arginine to L-ornithine and urea.[1] This protein plays important role in L-arginine homeostasis, regulating the level of L-arginine or L-ornithine, which is essential for various critical metabolic processes.[2,3] *H. pylori* contain RocF gene encoding arginase. It has been reported earlier that *H. pylori* arginase plays a critical role in providing acid resistance and thus is important for colonization of pathogen in the gastric epithelial cells.[4,5] It helps in evading the host immune response by down-regulating nitric oxide (NO) production from L-arginine by the inducible isoform of NO synthase (iNOS), as L-arginine is a common substrate for both iNOS and arginase.[6] It also plays a role in inhibiting T cell proliferation by down regulating the expression of CD3ζ.[7]

Mammalian and bacterial arginases have been studied extensively, and their 3D structures are available.[8−13] These proteins are found to exist as oligomers; mammalian arginases are generally trimer, whereas the bacterial counterparts are hexamer.[13] Arginases possess three conserved signature sequences GGDHS, SxDxDxxDP and DAHxD for binding to the metal ions, which are known to form a bimetallic center at the active-site.[13−15] The active-site of arginase containing two metal ions and a bridging hydroxide ion is shown in Figure 1. The nucleophilic attack by the bridging hydroxide between the two metal ions to the guanidine carbon of arginine is required for the hydrolysis reaction.[16] In contrast to other arginases, the *H. pylori* enzyme exists as a mixture of monomer and dimer,[17] suggesting that the mechanism of oligomerization in the *H. pylori* enzyme is different from other homologues.[9,13,16] *H. pylori* arginase possesses several distinct characteristics compared to other homologues which include (i) preference for Co^{2+} as a metal cofactor rather than Mn^{2+}, (ii) acidic pH optimum (6.1 instead of 9.5), (iii) cooperative mechanism of arginine hydrolysis, (iv) concentrations dependent self-association and activation, (v) significant sequence differences at the N- and C-terminal sites,[17,18] and (vi) presence of SSEHA sequence instead of GGDHS. Our recent studies illustrated the role of SSEHA sequence in the stability and activity of *H. pylori* arginase.[19] The

Received: October 18, 2012
Revised: December 24, 2012
Published: December 27, 2012

   dx.doi.org/10.1021/bi301421v | *Biochemistry* 2013, 52, 508−519

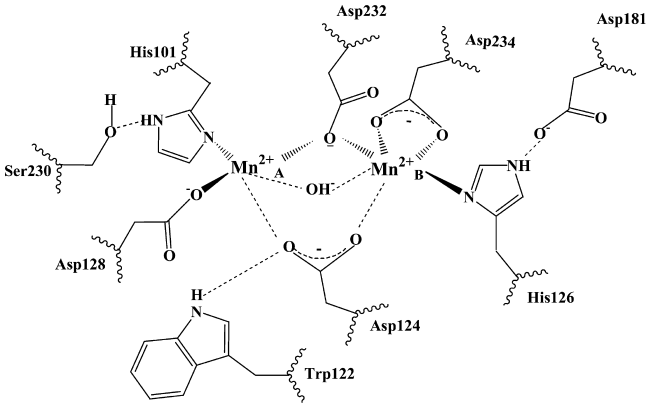

Figure 1. Representation of the active-site of human arginase I with first-shell metal residues His101, Asp232, Asp234, His126, Asp124, Asp128 and second-shell residues Asp181, Trp122, and Ser230 coordinating two metal ions (Mn^{2+}_{A} and Mn^{2+}_{B}) necessary for intact bimetallic cluster formation and L-arginine hydrolysis.

sequence analysis of the *H. pylori* enzyme clearly shows the presence of a unique 13 residues long sequence motif (^{153}ESEEKAWQKLCSL^{165}), which has not been found in any other arginase (Figure 2). On the basis of the previous report, the sequence motif was suggested to act as an anchor to the membrane.[5] In the absence of the 3D-structure of this protein, the model structures have been reported.[19,20] But the model structure did not provide appropriate insight into the role of this motif in the absence of the analogous sequence. Although the metal binding and other residues are conserved (Figure 2) in *H. pylori* arginase, we sought to investigate the role of the unique stretch of sequence motif which could provide structural and functional insight into this enzyme. Moreover, the increased interests for the search of arginase-based therapeutics and design of effective anticarcinogenic arginase from prokaryotes to eukaryotes have drawn considerable attention.[21] Various forms of human arginase I such as pegylated,[22] Co^{2+}-reconstituted[23] and the chimeric protein of human arginase I and human arginase II have been attempted to test the anticancer efficacy.[24−28] In the present report, we have undertaken a combination of approaches that include deletion of the sequence, kinetic assays, site-directed mutagenesis, metal analysis, circular dichroism, analytical gel-filtration assay, heat-induced denaturation and molecular dynamics (MD) simulations to investigate the location of the

```
Bacillus subtilis Arginase          AQKVNKVIEEKKFPLVLGGDHSIAIGTLAGTAKHYDN--LGVIWYDAHGD  124
Bacillus caldovelox Arginase        AAAVDQVVQRGRFPLVLGGDHSIAIGTLAGVAKHYER--LGVIWYDAHGD  126
Homo sapiens Arginase I             AGKVAEVKKNGRISLVLGGDHSLAIGSISGHARVHPD--LGVIWVDAHTD  128
Rattus norvegicus Arginase I        AAVVAETQKNGTISVVLGGDHSMAIGSISGHARVHPD--LCVIWVDAHTD  128
Homo sapiens Arginase II            AEVVSRAVSDGYSCVTLGGDHSLAIGTISGHARHCPD--LCVVWVDAHAD  147
Rattus norvegicus Arginase II       AEVVSRAVSGGYSCVTLGGDHSLAIGTISGHARHHPD--LCVIWVDAHAD  147
Helicobacter pylori Arginase        IPCMKEVFEKKEFPLILSSEHANMFGIFQAFRSVHKDKKIGILYLDAHAD  120
                                       : .. .     : *..:*:  :* : .         : ::: *** *

Bacillus subtilis Arginase          LNTLETSPSGNIHGMPLAVSLGIGHESLVNLE----------GYA--  159
Bacillus caldovelox Arginase        VNTAETSPSGNIHGMPLAASLGFGHPALTQIG----------GYS--  161
Homo sapiens Arginase I             INTPLTTTSGNLHGQPVSFLLKELKGKIPDVP----------GFSWV  165
Rattus norvegicus Arginase I        INTPLTTSSGNLHGQPVAFLLKELKGKFPDVP----------GFSWV  165
Homo sapiens Arginase II            INTPLTTSSGNLHGQPVSFLLRELQDKVPQLP----------GFSWI  184
Rattus norvegicus Arginase II       INTPLTTVSGNIHGQPLSFLIRELQDKVPQLP----------GFSWI  184
Helicobacter pylori Arginase        IHTAYDSDSKHIHGMPLGMVLNRVRSGFNRMSESEEKAWQKLCSLGLEKG  170
                                    ::*   : * ::** *:.  :   :  .  :            *

Bacillus subtilis Arginase          -PKIKPENVVIIGARSLDEGERKYIKESGMKVYTMHEIDRLGMTKVIEET  208
Bacillus caldovelox Arginase        -PKIKPEHVVLIGVRSLDEGEKKFIREKGIKIYTMHEVDRLGMTRVMEET  210
Homo sapiens Arginase I             TPCISAKDIVYIGLRDVDPGEHYILKTLGIKYFSMTEVDRLGIGKVMEET  215
Rattus norvegicus Arginase I        TPCISAKDIVYIGLRDVDPGEHYIIKTLGIKYFSMTEVDKLGIGKVMEET  215
Homo sapiens Arginase II            KPCISSASIVYIGLRDVDPPEHFILKNYDIQYFSMRDIDRLGIQKVMERT  234
Rattus norvegicus Arginase II       KPCLSPPNLVYIGLRDVEPAEHFILKSFDIQYFSMRDIDRLGIQKVMEQT  234
Helicobacter pylori Arginase        GLEIDPKCLVYFGVRSTEQSERDVIRELQIPLFSVDAI-RENMQEVVQKT  219
                                       :..  :* :* *. :  *:  ::   :  :::  : : .: .*::.*

Bacillus subtilis Arginase          LDYLSA--CDGVHLSLDLDGLDPNDAPGVGTPVVGGISYRESHLAMEMLY  256
Bacillus caldovelox Arginase        IAYLKER-TDGVHLSLDLDGLDPSDAPGVGTPVIGGLTYRESHLAMEMLA  259
Homo sapiens Arginase I             LSYLLGRKKRPIHLSFDVDGLDPSFTPATGTPVVGGLTYREGLYITEEIY  265
Rattus norvegicus Arginase I        FSYLLGRKKRPIHLSFDVDGLDPVFTPATGTPVVGGLSYREGLYITEEIY  265
Homo sapiens Arginase II            FDLLIGKRQRPIHLSFDIDAFDPTLAPATGTPVVGGLTYREGMYIAEEIH  284
Rattus norvegicus Arginase II       FDRLIGKRKRPIHLSFDIDAFDPKLAPATGTPVVGGLTYREGLYITEEIH  284
Helicobacter pylori Arginase        KESLKA--VDIIYLSLDLDIMDGKLFTSTGVRENNGLSFDELKQLLGLLL  267
                                       *       ::**:*:* :*    ...*.   .*::: *       :
```

Figure 2. CLUSTAL W alignment of *H. pylori arginase* (accession no. NP_208190) with *Bacillus subtilis* (accession no. BAA11291.1), *Bacillus caldovelox* (accession no. S68863), *Homo sapiens* arginase I (accession no. CAA31188.1), *Rattus norvegicus* arginase I (accession no. AAC22580.1), *Homo sapiens* arginase II (accession no. AAB39855.1), *Rattus norvegicus* arginase II (accession no. AAB06939.1). Highlighted areas indicate the amino acid signature motifs characteristics to the arginase family. Residues in bold are critical for the formation of a bimetallic cluster at the active-site. Nonconserved stretch of the sequence motif (153−165) is shown in the box. The N- and C-terminal residues are omitted for clarity.

dx.doi.org/10.1021/bi301421v | *Biochemistry* 2013, 52, 508−519

sequence motif and whether the entire sequence or its individual residue has impact on the kinetics, bimetallic site, structure, and stability of the protein. The study shows that the sequence displays a loop-cum-helix structure, which is located near the active-site. Our data also revealed that the protein became catalytically nonfunctional upon deletion of the sequence motif (Δ153−165). We identified key residues in this sequence that play critical roles in the function of the protein. We demonstrate that both Trp159 and Asp126 are individually crucial in maintaining a bimetallic center, and the interaction between these two residues appears to be important in positioning the motif near the active-site for activity. We also show that Cys163 is found to be crucial for dimerization of the protein. Although the sequence as a whole is important for the stability of the protein, Trp159 and Glu155 individually have a remarkable role in the stability. Thus, the present study not only provides significant new insights into the role of a nonconserved sequence motif in *H. pylroi* arginase but also offers a prospect of engineering this stretch of the sequence in other arginases for better anticarcinogenic agent against L-arginine auxotrophic tumors.

MATERIALS AND METHODS

Preparation of the Deletion Construct. The truncated construct (Δ153−165) of *H. pylori* arginase was prepared using two different sets of primers (Table S1, Supporting Information) with appropriate restriction enzyme sites to amplify the gene sequence present before and after insertion sequence. These amplified fragments were subsequently cloned into a GST-tagged pC6-2 vector sequentially. The deletion construct was confirmed by DNA sequencing.

Mutagenesis. Glu153Ala, Ser154Ala, Glu155Ala, Glu156Ala, Lys157Ala, Trp159Ala, Trp159Phe, Gln160Ala, Lys161Ala, Leu162Ala, Cys163Ala, Ser164Ala, and Asp126Ala of *H. pylori* arginase were generated using the QuickChange Site-Directed Mutagenesis kit (Stratagene, USA) according to the manufacturer's protocol. Appropriate forward and reverse primers (Table S1, Supporting Information) with GST-tagged pC6-2-rocF plasmid as a template were used for PCR reactions. The positive mutants were identified by DNA sequencing.

Protein Expression and Purification. Recombinant wild type and mutant proteins were expressed and purified following a reported procedure.[29] Briefly, the plasmid encoding rocF gene was transformed into *Escherichia coli* BL21 (DE3) pLys competent cells. The culture was induced with 0.1 mM isopropyl-β-D-thiogalactopyranoside for 12 h at 30 °C when OD_{600} reached to 0.6−0.8. EDTA-free protease inhibitor cocktail tablet (Roche Applied Science) containing 1× PBS buffer (137 mM NaCl, 2.7 mM KCl, 10 mM Na_2HPO_4, 2 mM KH_2PO_4, pH 7.2) was used for harvesting, resuspension and lysis of cells by French press (Thermo Electronics) at 1100 psi. Lysate was centrifuged at 14 000 rpm for 60 min and the supernatant was subjected to glutathione sepharose (Amersham) for affinity purification. Tag free protein was obtained by digesting the protein with purified caspase-6 as per the reported procedure,[30] and the protein was eluted with 1× PBS buffer. Caspase-6 was removed from the eluted fraction by passing onto a 1× PBS equilibrated 1-mL Ni-NTA agarose (Qiagen, CA) column. The protein was dialyzed against 20 mM Tris-HCl, pH 7.2 and then concentrated using centricon-10 at 4 °C and stored at −80 °C with 10% glycerol. The concentrations of the proteins were determined spectrophotometrically using Bradford assay. The deletion protein was expressed and purified similar to wild type. All individual mutants including wild type were free from the tag and were used for the kinetic, metal analysis, and biophysical experiments.

Activity Assay. The arginase activity assay of apo- and holoproteins was carried out spectrophotometrically as reported earlier[17] by measuring the formation of ornithine at 515 nm with ninhydrin. The activity assay of the EDTA-free apoprotein confirmed the requirement of the metal cofactor for activity. The assay was carried out at 20 mM Tris-HCl, pH 7.2. The ratio of the concentration of the metal to the protein with optimum activity was determined for WT and each mutant. For wild type, the ratio was found to be 20:1 and 500:1 for Co^{2+} and Mn^{2+} respectively. The ratio was found to increase with a few mutants and was used for the kinetic assays.

Kinetic Analysis. The steady-state kinetic assays were carried out with metal incubated apoprotein using a reported procedure.[17] The assays were done with both the Co^{2+}- and Mn^{2+}-reconstituted mutant proteins in order to examine their metal preference. The reactions were carried out by mixing the metal incubated apoprotein with varying concentrations of arginine. In these assays, the substrate was used in large excess over the enzyme so that multiple turnovers could be studied. For all experiments, the initial rate for the formation of L-ornithine was measured. The experimental data under the above conditions were fitted to a Hill equation using Sigmaplot (version 10) to obtain the steady-state kinetic parameters as reported earlier.[17]

Gel-Filtration Chromatography. Analytical gel-filtration assay was carried out using a Perkin-Elmer HPLC system, USA. 10 μM of protein was injected into a Phenomenex S-4000 column with 20 mM Tris-HCl, pH 7.2 at a flow rate of 1 mL/min. A standard curve was generated from the elution volumes of proteins with known molecular mass such as amylase (200 kDa), alcohol dehydrogenase (150 kDa), bovine serum albumin (66 kDa) and carbonic anhydrase (29 kDa) and the molecular mass of the protein was calculated from the retention volume.

Metal Analysis. For metal analysis, 1−2 μM apoprotein was incubated with excess Co^{2+} and Mn^{2+} ions (50 °C for 30 min) for WT and mutants. Unbound metal was removed by passing through Sephadex G-25 columns equilibrated with 20 mM Tris, pH 7.2. The flow through was used for the metal analysis following the reported [4-(2-pyridylazo) resorcinol] (PAR) assays[19,31] with 6 M guanidine hydrochloride using a standard curve with known metal concentrations. The absorbance of the complex for Co^{2+} and Mn^{2+} was measured at 515 and 495 nm respectively after 30 min of incubation at room temperature. The experiment was carried out in triplicate for each metal ion.

MD Simulations. The model structure of *H. pylori* arginase contains two cobalt atoms at its active-site.[19] To refine this, the MD simulations were carried out in the absence of the metal ions. The simulation was carried out using double precision GROMACS 4.5.4 with Charmm27 force field. The protein was solvated with 24972 Tip3p water molecules in a cubical box of dimension 9.27 × 9.27 × 9.27 nm^3. In order to simulate cellular aqueous medium 0.1 M NaCl was included in addition to 6 Na^+ ions which is required for neutralizing the system. Then the system was subjected to steepest descent energy minimization down to a gradient of 1000 kJ $mole^{-1}$ nm^{-1}. Thereafter the simulation was done in two steps. The first step was a 100 ps position restraint dynamics using LINCS algorithm for allowing the water molecule to move freely around restrained (partially frozen) atoms of protein molecule. This permits the equilibration and free diffusion of solvent molecule into the protein molecules. In the next step full 450 ns production run was carried out at 300

Table 1. Steady-State Kinetic Parameters of Wild Type and Mutant *H. pylori* Arginases[a]

	Co^{2+}-reconstituted			Mn^{2+}-reconstituted		
protein	k_{cat} (min^{-1})	$K_{0.5}$ (mM)	n	k_{cat} (min^{-1})	$K_{0.5}$ (mM)	n
wild type	31 ± 2.8	6.2 ± 0.5	1.8 ± 0.1	10 ± 0.9	7.1 ± 0.6	1.6 ± 0.2
Glu153Ala	16.2 ± 0.6	4.3 ± 0.3	2.1 ± 0.3	2.3 ± 0.04	1.8 ± 0.14	1.7 ± 0.1
Ser154Ala	18.7 ± 0.8	4.6 ± 0.4	2.2 ± 0.4	1.3 ± 0.1	3.2 ± 0.8	1.5 ± 0.5
Glu155Ala	N.A.	N.A.		N.A.	N.A.	
Glu156Ala	14.2 ± 0.6	14.4 ± 0.9	1.8 ± 0.1	N.A.	N.A.	
Lys157Ala	14.7 ± 0.7	4.0 ± 0.4	1.7 ± 0.2	10.7 ± 1.0	7.2 ± 0.6	2.0 ± 0.3
Trp159Ala	N.A.	N.A.		N.A.	N.A.	
Trp159Phe	N.A.	N.A.		N.A.	N.A.	
Gln160Ala	14.7 ± 1.8	12.1 ± 2.0	1.7 ± 0.2	2.7 ± 0.2	31.5 ± 3.0	
Lys161Ala	108.4 ± 4.3	4.2 ± 0.3	1.8 ± 0.2	29.9 ± 1.1	5.0 ± 0.3	2.2 ± 0.2
Leu162Ala	67.9 ± 5.5	10.6 ± 1.3	1.6 ± 0.2	12.8 ± 1.1	18.9 ± 3.2	1.1 ± 0.1
Cys163Ala	1.9 ± 0.2	5.9 ± 1.5	1.2 ± 0.2	N.A.	N.A.	
Ser164Ala	14.3 ± 0.5	3.9 ± 0.3	2.1 ± 0.4	3.2 ± 0.2	4.3 ± 0.7	1.2 ± 0.1
Asp126Ala	N.A.	N.A.		N.A.	N.A.	

[a]N.A. - no activity observed, 0.05% of wild type activity or below was considered to be "no activity observed". The concentration of the apo-protein was 1 μM. The ratio of the concentration of the metal to the protein was determined for wild type and mutants, where highest activity was observed. For wild type, the ratio was found to be 20:1 and 500:1 for Co^{2+} and Mn^{2+} respectively. For each mutant this ratio was determined and used for the kinetic assays. The data were analyzed using a Hill equation, rate = $k_{cat}\cdot[E_0]\cdot[Arg]^n/(K_{0.5}{}^n + [Arg]^n)$ and the kinetic parameters apparent $K_{0.5}$, k_{cat}, and n (Hill co-efficient) were determined. The quality of the fit was checked by a theoretical line drawn through the experimental data points and highest confidence limit. The assays were carried out with the tag free proteins.

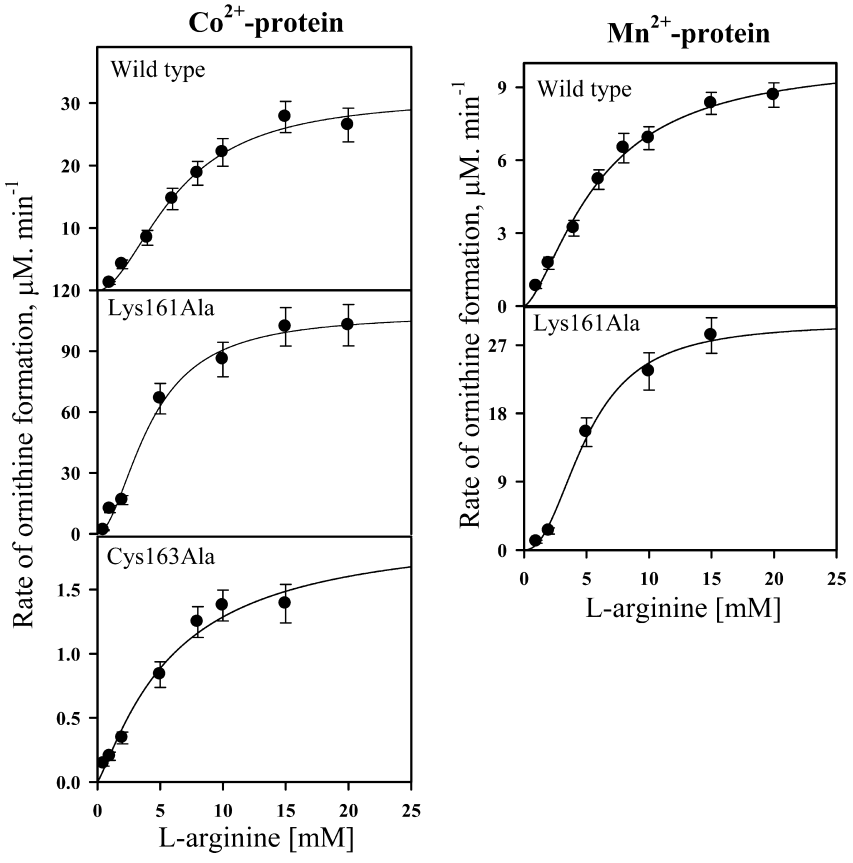

Figure 3. Steady-state kinetic analysis showing the representative plots of wild type and mutant proteins in the presence of Co^{2+} or Mn^{2+}. The data were fitted to a sigmoidal equation, rate = $k_{cat}\cdot[E_0]\cdot[Arg]^n/(K_{0.5}{}^n + [Arg]^n)$ yielding $K_{0.5}$, k_{cat}, and n (Hill coefficient). Cys163Ala did not show detectable activity in the presence of Mn^{2+} and hence its plot was not shown. The kinetic parameters were shown in Table 1. The quality of the fit was judged by a theoretical line drawn though the experimental data, standard error and confidence limit.

K. All the simulations were carried out at standard pressure of 1 bar with a coupling constant of 0.5 ps for pressure and 0.1 ps for temperature making use of Brendsen coupling algorithm in both cases. The time step for the integration algorithm was kept at 2 fs. PME electrostatics was applied using a Lennard-Jones cutoff of 1.4 nm and coulomb cutoff of 0.9 nm. The maximum spacing for the Fast Fourier transform grid was kept at 0.12 nm and cubic interpolation order was applied. Snapshots of the MD trajectory

dx.doi.org/10.1021/bi301421v | *Biochemistry* 2013, 52, 508−519

were saved at each 100 ps. The model structure discussed here is a snapshot at 445.7 ns. The secondary and tertiary structures were evaluated by Ramachandran plot, as most of the residues are found in the allowed regions (Figure S1, Supporting Information). Several loops are found to be flexible (Figure S2, Supporting Information).

Docking Studies. Docking study of *H. pylori* arginase with nonsimulated and simulated structures was done with substrate L-arginine using Autodock 4.2. Blind docking on rigid protein models with flexible arginine molecule was carried out using Lamarkian Genetic algorithm. The substrate was allowed to explore their conformational space while the protein models were kept constant. A grid size of 62 Å × 62 Å × 62 Å with docking parameter of population size 250, number of energy evaluation 2500000 and number of Lamarkian Genetic algorithm run of 200 was used. The default clustering parameters were used. The lowest energy conformation of the largest cluster was treated as the best docked structure.

Circular Dichroism Measurement and Heat-Induced Denaturations. Circular dichroism (CD) spectra of apo- and Co^{2+}-reconstituted wild type and mutant proteins in the far-UV range were recorded on a Jasco J-815 spectropolarimeter using a 1-mm path length cuvette. All spectra were corrected by subtracting the baselines of buffer and buffer plus metal ion, recorded under the same condition. The measurements were done using 20 mM Tris, pH 7.2. For the determination of T_m the sample was heated at the rate of about 1 °C/min, and the data were recorded at the interval of 5°. The temperature of sample was raised from 30° to 90 °C using a peltier thermostat, coupled with the spectropolarimeter. To calculate the melting temperature, θ_{MRW} at 220 nm values were plotted against temperature and the data were fitted using a two-state unfolding model. To check the reversibility, the protein was thermally denatured (temperature was kept higher than the T_m) and cooled down to the room temperature, and it was reheated. Similar thermal denaturation profile and T_m were obtained, suggesting that unfolding occurs in a reversible manner.

RESULTS

Mutational Studies on the Sequence Motif. Unlike other arginases, the *H. pylori* enzyme has been reported to show higher activity with Co^{2+} than Mn^{2+}.[17] *H. pylori* arginase has a distinct sequence motif ^{153}ESEEKAWQKLCSL^{165}, which is absent in the analogous enzymes (Figure 2). To examine the role of the sequence, each residue was individually mutated with alanine and the kinetic assays were carried out. Similar to wild type, the data were fitted to a sigmoidal equation to evaluate the kinetic parameters $K_{0.5}$ (an apparent affinity for the substrate to the enzyme, for allosteric protein K_m is represented as $K_{0.5}$), k_{cat} (catalytic rate) and n (Hill coefficient or degree of cooperativity), which are shown in Table 1. A plot for the steady-state kinetic analysis of wild type protein is shown in Figure 3. Comparison of the $k_{cat}/K_{0.5}$ (apparent catalytic efficiency) values (Figure 4) showed that like wild type, the mutant proteins showed highest activity with Co^{2+} as a metal cofactor, consistent with Co^{2+} being a preferred metal ion.

Among the mutants, Glu155Ala, Trp159Ala, and Cys163Ala showed remarkable results (Table 1). Glu155Ala and Trp159Ala resulted in complete loss of the catalytic activity, demonstrating that these two residues are extremely critical for the function of the protein (see the discussion of metal binding studies). Cys163Ala showed a decrease in the catalytic efficiency by about 16-fold compared to the wild type in the presence of Co^{2+}.

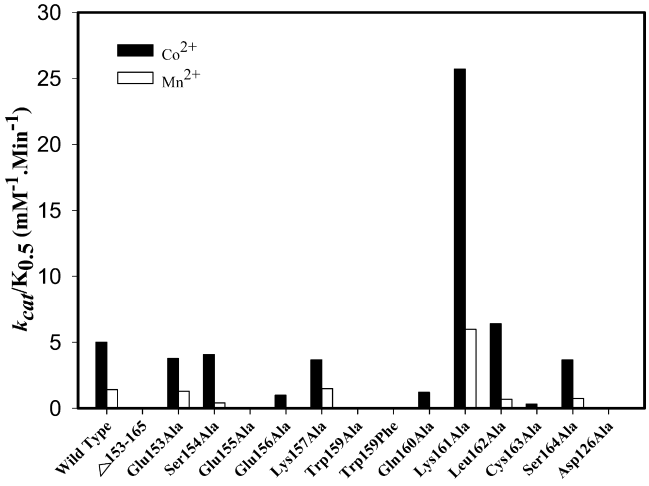

Figure 4. The apparent catalytic efficiency ($k_{cat}/K_{0.5}$) of the wild type and mutant *H. pylori*. The assay was carried out with a preincubated reaction mixture containing 1 μM apoenzyme and 20 μM Co^{2+} or 500 μM Mn^{2+} ions with varying concentrations of L-arginine for the wild type protein, since this concentration of the wild type apoenzyme to the metal ions showed optimal activity for Co^{2+} and Mn^{2+} respectively. The data were analyzed using a Hill equation, rate = $k_{cat}\cdot[E_0]\cdot[Arg]^n/(K_{0.5}{}^n + [Arg]^n)$ and the kinetic parameters apparent $K_{0.5}$, k_{cat}, and n (Hill coefficient) were determined. The quality of the fit was checked by a theoretical line drawn through the experimental data points and highest confidence limit. The ratio of the metal ions to the apoenzyme was determined for each mutant where highest activity was observed, and this was used for the steady-state kinetic assays. The experiments were done in triplicate.

However, with Mn^{2+} Cys163Ala failed to show detectable activity indicating that Cys163 is also critically important for catalysis. The steady-state kinetic analysis for some of the mutants is shown in Figure 3. $K_{0.5}$ value for majority of the mutants is similar to wild type except for a few cases (Table 1). However, for Glu156Ala, Gln160Ala, and Leu162Ala, $K_{0.5}$ increased by ∼2-fold implying that these residues have some effects for the substrate binding. Interestingly, k_{cat} varies with mutations highlighting the impact of the sequence motif in catalysis. The catalytic efficiency for Glu156Ala decreased by ∼5 fold than the wild type suggesting that Glu156 is also important for the function of the protein (Figure 4). The decrease in the catalytic efficiency in this mutant is because of the decrease in the affinity of the substrate as well as for a decrease in the catalytic rate (Table 1). With Mn^{2+} Glu156Ala did not exhibit detectable activity, further suggesting the role of Glu156 in the function (Figure 4). Similar to Glu156Ala, Gln160Ala also showed a decrease in the catalytic efficiency by ∼5-fold. In contrast, Lys161Ala displayed ∼5 fold increase in the catalytic efficiency compared to wild type indicating that this residue is important in modulation of the activity. Other residues did not show significant difference in the efficiency compared to wild type.

In allosteric protein, the value of n obtained in the Hill equation provides the degree of cooperativity. Our kinetic analysis suggests that Cys163 ($n \sim 1.2$) is likely to be a key residue for oligomerization of the protein. To investigate this, we have carried out analytical gel-filtration assays on wild type protein as well as on Cys163Ala. Analysis of the data showed that wild type protein eluted as a mixture of monomer and dimer with similar proportion (Figure 5), which is consistent with the reported result.[17] Interestingly, Cys163Ala eluted mainly as a monomer with dimer being a smaller amount (Figure 5),

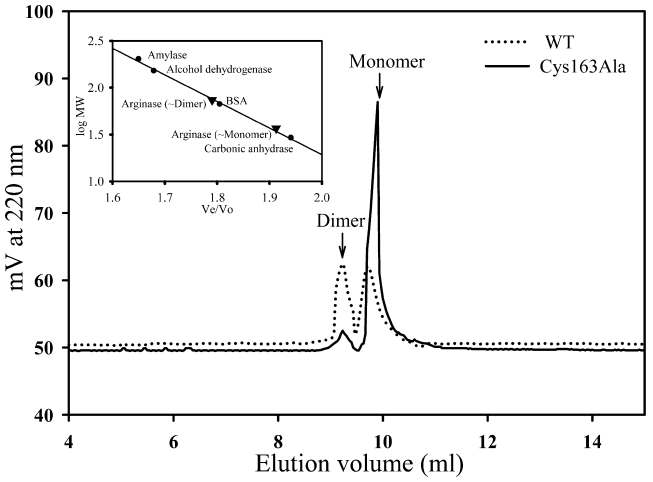

Figure 5. Analytical gel-filtration assay showing the elution profiles of wild type and Cys163Ala. The assay was carried out in 20 mM Tris-HCl, pH 7.2. Inset shows a curve using protein standards. The higher retention volume corresponds to molecular mass of ~34.2 kDa, consistent with a monomer (calculated mass of a monomer ~ 36.9 kDa), whereas the smaller one with a molecular mass of ~75.9 kDa corresponds to a dimer (calculated mass of a dimer ~ 73.8 kDa).

indicating that Cys163 plays a critical role in dimerization of the protein. Thus, the kinetic assays in combination with the gel-filtration analysis demonstrate that the motif is extremely critical for the function of the protein.

Simulations Studies and Location of the Sequence Motif. The model structure of *H. pylori* arginase with respect to its closest homologue *Bacillus caldovelox* enzyme suggested that the sequence motif is far from the active-site and exposed to the solvent.[19,20] MD simulation in explicit solvent for proteins is one of the methods that have been used for the refinement of low resolution homology models.[32−39] To get a structural insight into how the motif is important for the function of the protein, we have done the MD simulations to refine the reported model structure of *H. pylori* arginase. The protein backbone RMSD values showed equilibrium structures after 400 ns of simulations (Figure 6A). Figure 6B represents a snapshot of the simulated structure at 445.7 ns. To further validate our simulations, the docking studies of the simulated structure with the substrate L-arginine was carried out (Figure S3, Supporting Information). The binding energy was found to be favorable with the simulated structure as compared to the reported model structure (−5.93 vs 0.68 kcal/mol), suggesting that the simulated structure can provide a better insight into the function of the protein. Figure 6B also shows the overlay of the simulated and reported model structures of *H. pylori* arginase. Interestingly, there is a variation in the structure and positioning of the motif. The simulated structure shows that the sequence consists of largely a loop with a small helix in Lys161-Ser164 (Figure 6C). Trp159 moved closer to the metal binding site and is buried in the protein. As observed in Figure 7B, the positioning of the motif near the active-site is due to the hydrogen bonding interaction of Trp159 with Asp126 (distance ~2.65 Å). This interaction was formed at around 120 ns and remained intact during rest of the simulations (Figure 7A), implying that it may have an impact on the structure and function of the protein. To verify this, Asp126 was mutated to Ala and the kinetic assay was done. Interestingly, this mutant resulted in complete loss of the catalytic activity, indicating that Asp126 is vital for the function. As shown in the mutational study, Trp159Ala failed to show detectable activity. The data further suggest that the interaction of Trp159 with Asp126 appears to be critical in positioning the motif near the active site for the function of the protein (Figure 7B and Table 2 for metal analysis). It is also to be noted that the location of the active-site residues is not primarily altered. Thus, the MD simulations results show that the sequence motif is located near the active-

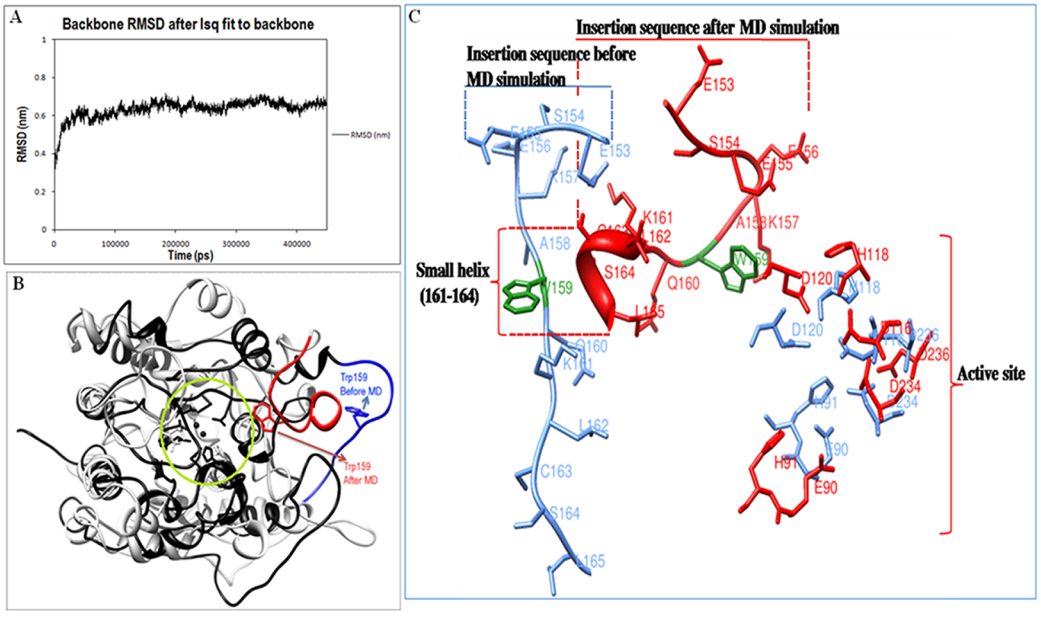

Figure 6. (A) The backbone RMSD value after least-squares fit with backbone of initial structure during 450 ns MD simulation of the model without metal atom. (B) Overlap of *H. pylori* arginase model structure (gray) and the structure obtained after 450 ns of MD simulation (black). The active-site is shown in green circle, whereas the sequence motif is shown in blue (before simulation) and red (after simulation). The location of Trp159 is shown after and before simulations. (C) Sequence motif and the active-site of *H. pylori* arginase in the nonsimulated (sky blue) and simulated structures (red). Trp159 in both the structures is shown in green.

dx.doi.org/10.1021/bi301421v | *Biochemistry* 2013, 52, 508−519

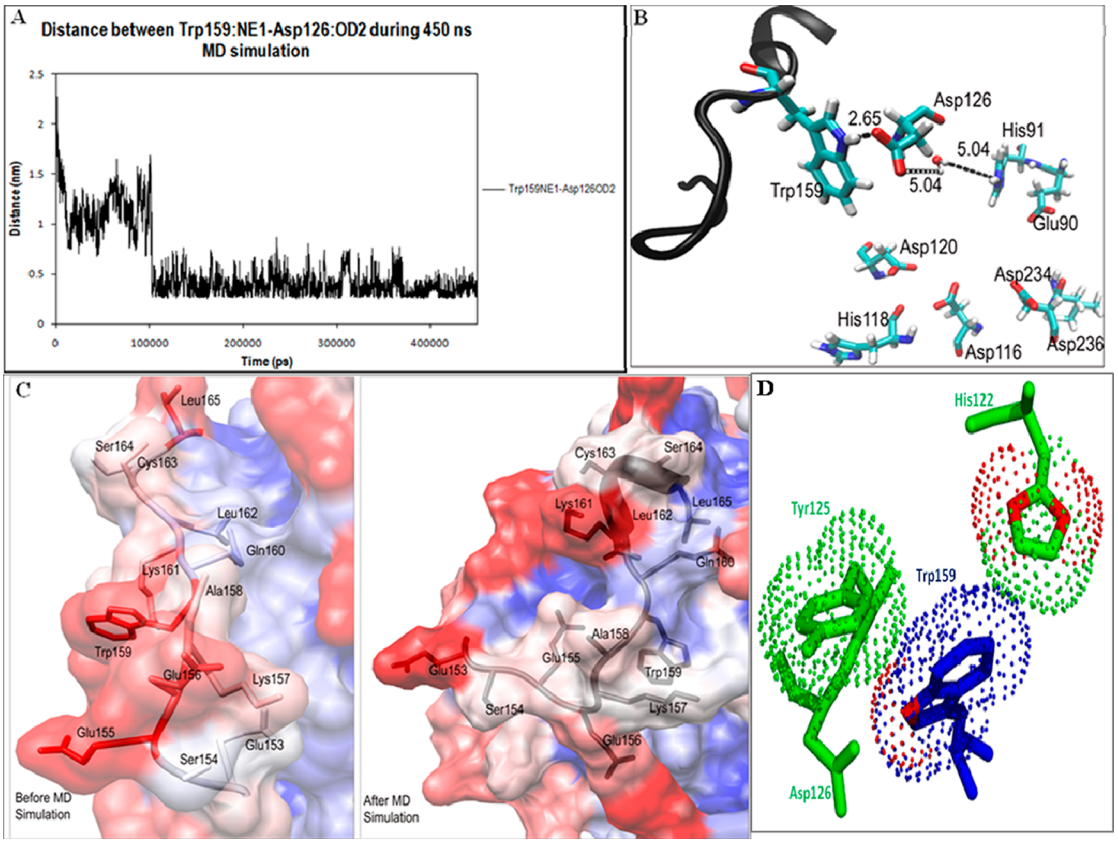

Figure 7. (A) The distance between Trp159 and Asp126 is shown during MD simulation. This distance decreases to a length where the bond formation is possible and remains unaltered throughout the trajectory after 100 ns. (B) The distance between Trp159-Asp126 is shown in one of the snapshot of MD trajectory. (C) Surface representation of the residues for the sequence motif in *H. pylori* arginase using solvent accessible surface area (SASA) value before and after MD simulations. The exposure of the residues decreases from red to white to blue (red, white and blue represent exposed, less exposed and buried, respectively). (D) The electron clouds of Trp159 with Tyr125 and His122 within the van der Waal's distance showing the stabilization of the protein by Trp159 with the surrounding aromatic amino acids through hydrophobic and/or $\pi-\pi$ interactions.

Table 2. Metal Content in the Co^{2+}- and Mn^{2+}-Reconstituted Wild Type and Mutant *H. pylori* Arginases

protein	number of Co^{2+} per monomer	number of Mn^{2+} per monomer
wild type	2.1 ± 0.1	2.2 ± 0.1
Glu153Ala	1.6 ± 0.2	2.0 ± 0.1
Ser154Ala	2.0 ± 0.1	2.1 ± 0.2
Glu155Ala	1.6 ± 0.1	2.0 ± 0.1
Glu156Ala	1.6 ± 0.2	2.1 ± 0.2
Lys157Ala	1.6 ± 0.1	1.9 ± 0.1
Trp159Ala	1.1 ± 0.2	1.1 ± 0.1
Trp159Phe	1.0 ± 0.2	0.9 ± 0.1
Gln160Ala	1.6 ± 0.2	1.7 ± 0.2
Lys161Ala	1.7 ± 0.2	2.2 ± 0.1
Leu162Ala	1.8 ± 0.1	1.9 ± 0.2
Cys163Ala	1.8 ± 0.2	1.8 ± 0.2
Ser164Ala	1.7 ± 0.1	2.2 ± 0.1
Asp126Ala	1.1 ± 0.2	1.2 ± 0.2

site with a loop-cum-helix structure, suggesting its role in both structure and function of the protein.

Evaluation of the Metal Binding upon Mutations. To examine whether the change in the catalytic activity is due to the alteration in the metal binding, the metal binding assay was carried out in all mutant proteins. As already known, in all arginases an intact bimetallic center at the active-site is absolutely essential for catalysis. Like wild type, all mutants except Trp159Ala exhibit similar metal binding (~2 metals per unit monomer of the protein) in the presence of either Co^{2+} or Mn^{2+} consistent with a bimetallic center at the active-site (Table 3). Trp159Ala is found to have one metal per unit monomer of the protein, suggesting that Trp159 is crucial in retaining a metal ion. To verify this, Trp159 was mutated with a similar hydrophobic residue Phe. Like Trp159Ala, Trp159Phe also showed no detectable activity (Figure 4) and contains one metal ion (Table 3), further verifying that Trp159 is critical in retaining a metal ion and thus in the activity. To understand whether Asp126 has a role in retaining metal ions, we carried out similar analysis for Asp126Ala in the presence of either Co^{2+} or Mn^{2+}. Interestingly, Asp126Ala also showed one metal ion, indicating that Asp126 is crucial for retaining a metal ion. These studies demonstrate that both Trp159 and Asp126 are close to the metal binding/active-site and critical for retaining the bimetallic center, thus for the function of the protein, which is consistent with the kinetic assays and MD simulations.

Deletion Studies on the Sequence Motif. Our studies so far show that Glu155, Trp159, Cys163 and Asp126 are critical for the function of the protein. To examine the role of the whole sequence motif in the activity, we have made a truncated *H. pylori* arginase, where the residues 153−165 have been deleted. Unlike wild type and mutant proteins, the GST-tag could not be cleaved in the truncated protein using caspase-6 indicating that the cleavage site may be buried inside the fused protein. The activity assay of the GST-tagged truncated protein was carried out. As

dx.doi.org/10.1021/bi301421v | *Biochemistry* 2013, 52, 508−519

Table 3. Melting Temperature (T_m) of Wild Type and Mutant *H. pylori* Arginases[a]

protein	apo-enzyme T_m (°C)	holo-enzyme T_m (°C)
Wild Type	68.0 ± 1.2	70.0 ± 0.4
Glu153Ala	58.4 ± 1.0	69.8 ± 2.1
Ser154Ala	59.5 ± 0.5	69.0 ± 1.0
Glu155Ala	53.6 ± 0.6	61.7 ± 2.4
Glu156Ala	59.0 ± 0.9	N.D.
Lys157Ala	57.7 ± 1.1	67.7 ± 0.5
Trp159Ala	51.0 ± 2.7	N.D.
Trp159Phe	59.9 ± 0.3	64.8 ± 1.3
Gln160Ala	62.8 ± 0.7	64.4 ± 1.0
Lys161Ala	59.0 ± 0.2	67.5 ± 0.5
Leu162Ala	61.0 ± 2.0	67.3 ± 0.9
Cys163Ala	60.5 ± 0.7	69.5 ± 0.7
Ser164Ala	59.9 ± 1.3	70.7 ± 1.8
Asp126Ala	61.0 ± 4.7	N.D.

[a]N.D. - not determined, these mutants did not show proper thermal transitions in the presence of the metal ions and hence their T_m values could not be determined reliably. The T_m was determined from the heat-induced denaturation studies on the apo and mutant Co^{2+}-proteins. The concentration of the protein was 1.5 μM for both apo and holo proteins. The experiments were carried out by measuring the CD spectra at 200−240 nm using a 1 mm path length cuvette in 20 mM Tris-HCl, pH 7.2. θ_{MRW} values at 220 nm were plotted against temperature and the T_m was calculated by fitting the data to a two-state model.

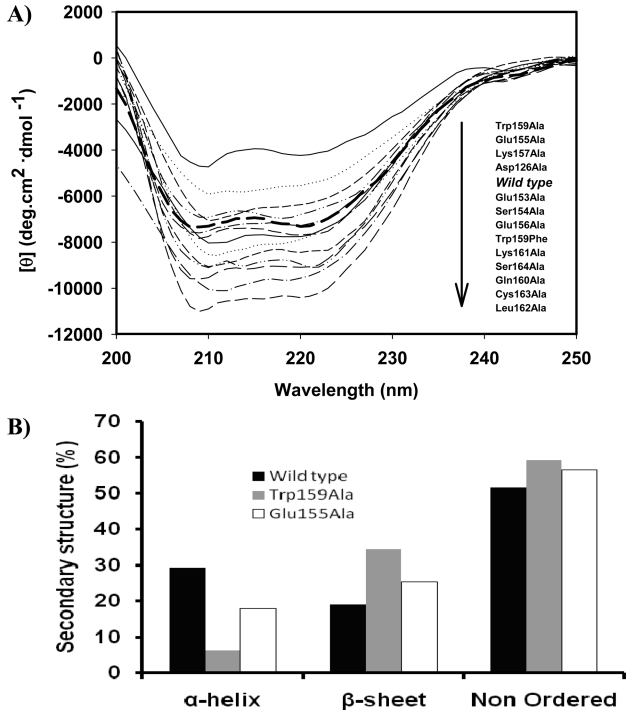

Figure 8. (A) CD measurement of the mutant proteins in the absence of the metal ions. The concentrations of the proteins were kept at 1.5 μM and the data were collected before the saturation of high voltage. (B) The representative secondary structure analysis of wild type, Trp159Ala and Glu155Ala by K2D3 and the Chen method.

obvious, the protein failed to display activity (Figure 4), further implying that the sequence motif is critical for the function of the protein. It is to be noted that the wild type protein is found to show similar activity with and without the tag.

Circular Dichroism Study for the Role of the Sequence in Secondary Structure. To examine the role of the sequence motif in the secondary structure of the protein, we employed CD measurements in the far UV range. The experiments were carried out for the wild type and mutants (apo and holo). For the apo proteins, the CD value was found to change for certain mutations (Figure 8A). Trp159Ala and Glu155Ala showed significant decrease in the CD value compared to wild type (Figure 8A), suggesting that these mutations lead to the loss of secondary structure of the protein. The deconvolution of the CD spectra by two different methods K2D3[40] and Chen[41] yielded an average α-helix content of ∼6.3 and 18% for Trp159Ala and Glu155Ala, respectively as compared to 29% in wild type (Figure 8B). To understand whether Trp159 is important for the secondary structure of the protein, we carried out similar studies with Trp159Phe. In contrast to Trp159Ala, Trp159Phe regained the secondary structure. These data demonstrate that both Trp159 and Glu155 of the motif are individually important for maintaining the structure of the protein. But Glu153Ala, Ser154Ala, Glu156Ala and Asp126Ala exhibit similar secondary structures to wild type. On the other hand, Gln160Ala, Lys161Ala, Leu162Ala, Cys163Ala and Ser164Ala showed an increase in the CD value compared to wild type. The increase in the helicity of these mutants may be due to the presence of Ala, which is known to have higher propensity to form helical structure.

To understand whether the loss of activity in Glu155Ala is due to the decrease in the helical content, CD measurement of Glu155Ala was carried out in the presence of 5−10% trifluoro ethanol (TFE), a known α-helical structure inducing agent in protein. The secondary structure of the mutant was found to increase with TFE (Figure S4, Supporting Information). Glu155Ala with 10% TFE exhibited a CD value similar to wild type, indicating that TFE increases the secondary structure of the mutant protein. To examine whether the structural gain in Glu155Ala with TFE makes the protein catalytically functional, the activity assay was carried out in the presence of 10% TFE. The mutant showed negligible activity (∼2% of wild type), suggesting that Glu155 has also a catalytic role.

To understand whether the metal ions have a role in the secondary structure of the mutant proteins, similar CD measurements were carried out. In the presence of the metal ions, the CD values of Glu153Ala, Ser154Ala, Lys157Ala, Trp159Ala, Trp159Phe, and Lys161Ala are found to be higher than their apos, indicating that the metal ions increase the secondary structure of these mutant proteins (data not shown). However, for other mutants the increase in the CD values is marginal in the presence of the metal ions.

Heat-Induced Denaturation Studies for the Role of the Sequence in Stability. To determine whether the sequence motif is important for the stability of the protein, heat-induced unfolding studies were carried out in all mutants using CD measurements. The change in the secondary structure was measured with an increase in the temperature from 30 to 90 °C, and the data were plotted against temperature. Figure 9A shows a representative plot of heat-induced unfolding studies in apoprotein. The data were fitted to a two-state unfolding model to determine the T_m (midpoint transition temperature), as shown in Table 3. All mutants showed sigmoidal transitions suggesting that temperature induced unfolding of the proteins occurred in a cooperative manner. The value of T_m of a protein provides an estimate for measuring its thermostability. Comparison of the T_m values between the wild type and mutants

dx.doi.org/10.1021/bi301421v | *Biochemistry* 2013, 52, 508−519

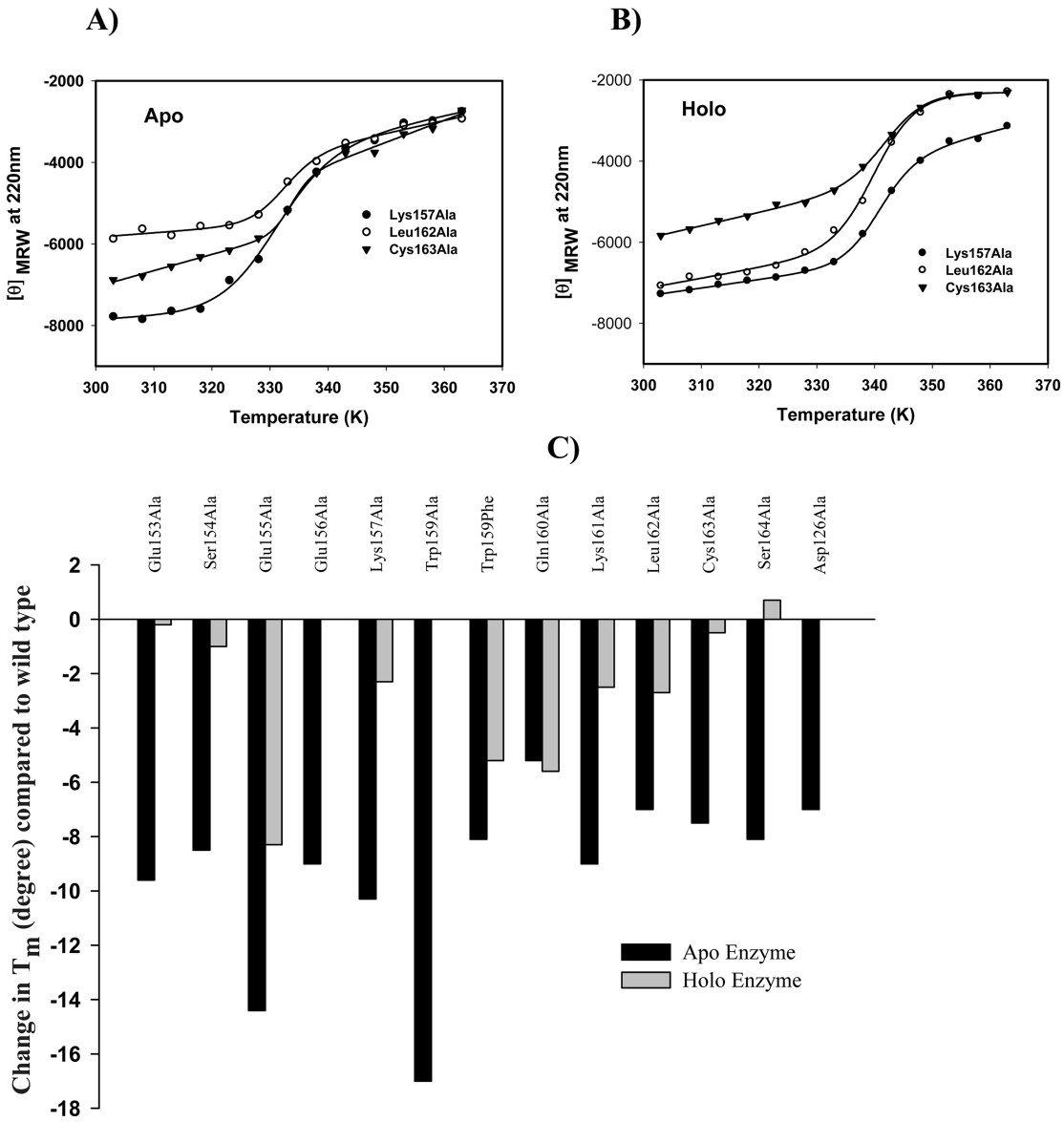

Figure 9. (A) Representative heat-induced transitions for apo Lys157Ala, Leu162Ala and Cys163Ala by CD measurement. Data were fitted to a two-state model to determine the T_m (B) Representative heat-induced transitions for Co^{2+}-reconstituted Lys157A, Leu162Ala and Cys163Ala by CD measurement and the data were fitted as mentioned above to determine the T_m, (C) The T_m of individual mutants was determined for both apo and holo forms as described in panels A and B. T_m of each mutant protein for both apo and holo forms were subtracted from WT and the difference in the T_m of the mutant proteins compared to wild type was plotted for apo and holoproteins.

showed that in the absence of the metal ions the mutant proteins are significantly less stable than the wild type, as reflected in the reduction of the T_m by ~5−17° (T_m of wild type apo ~68 °C, Figure 9C). Interestingly, only Glu155Ala and Trp159Ala showed the notable decrease in the T_m (~14−17°, Figure 9C) compared to wild type, suggesting that both electrostatic (by Glu155) and hydrophobic (by Trp159) interactions are very critical in providing stability to the apo-proteins. But Trp159 has a slightly larger role in the stability than Glu155, as observed from the difference in the T_m values compared to wild type (17 vs 14°). Tryptophans are found to increase the stability of proteins through hydrophobic and $\pi-\pi$ interactions with the side chains of aromatic amino acids.[42,43] To see the involvement of Trp159 in these interactions, the stability of Trp159Phe was examined. The data showed an increase in the T_m of about 9 deg as compared to Trp159Ala (60 vs 51 °C), suggesting the role of Trp159 in the hydrophobic and/or $\pi-\pi$ interactions for the stability of the protein (see the Discussion).

To see the effect of the metal ions in the stability, similar measurements were done on the mutant proteins in the presence of the metal ions and their T_m values were also evaluated (Figure 9B). As observed in Figure 9C, the interaction of the metal ions with the residues at the active-site compensates for the loss of stability in the mutant proteins. Unlike other mutants, the metal ions in Glu155Ala did not compensate the loss of stability significantly compared to their apos, suggesting that the interaction of Glu155 with its surrounding residues is vital for the stability of the protein. But for Trp159Phe, the loss of one metal as well as absence of the Trp159−Asp126 interaction is likely to be the main reasons for not regaining the stability. Thus, the heat-induced unfolding studies clearly demonstrate that the sequence motif is a critical component for the stability of *H. pylori* arginase.

dx.doi.org/10.1021/bi301421v | *Biochemistry* 2013, 52, 508−519

DISCUSSION

Although the first-shell and second-shell residues are primarily conserved in arginases for an intact bimetallic center at the active-site to carry out the hydrolysis reaction of L-arginine, the evolutionary role of a distinct sequence motif in the *H. pylori* enzyme remains unknown. The model structure of this protein with respect to its closest homologue showed that the sequence motif was far from the active-site and exposed to the solvent.[19,20] In the present study we have undertaken a number of approaches to demonstrate that the sequence motif is located near the active-site and indeed a critical component of the protein for structure, function, stability, and retention of bimetallic center.

H. pylori arginase shows several distinct features compared to the homologous enzymes.[17,18,44] One of the important features is that it exists as a mixture of monomer and dimer, and dimer has been shown to be important for stimulation of the activity through allosteric interaction.[17] The kinetic data showed that majority of the mutant proteins exhibit cooperativity, indicating that the mutants possess similar stimulation like wild type protein. Cys163Ala showed significant decrease (~16-fold) in the catalytic efficiency compared to wild type and did not show appreciable cooperativity ($n \sim 1.2$). Hence, the decrease in the catalytic efficiency of Cys163Ala is due to the absence of allosteric interaction. This is supported by the analytical gel-filtration assays, where Cys163Ala predominantly exists as a monomer. The MD simulations have clearly indicated that Cys163 of a small helix (Lys161-Ser164) is exposed to the solvent. Taken together, our data demonstrate that Cys163 is critical for dimerization of the protein. Unlike in the presence of Co^{2+}, Leu162Ala and Ser164Ala do not exhibit cooperativity with Mn^{2+} ($n \sim 1.1$), implying that these residues are also important in the regulation of the activity. The absence of cooperativity in these Mn^{2+} mutant proteins compared to Co^{2+} may due to the difference in subtle conformational change around the metal ions, as wild type Co^{2+}- and Mn^{2+}- *H. pylori* arginases have been found to exhibit different local tertiary structures.[17] The increase in the catalytic efficiency for Lys161Ala could be due to the increase in the catalytically competent conformation of the protein, as the secondary structure and stability of the mutant did not alter significantly compared to wild type in the presence of the metal ions. Nevertheless, our kinetic data in combination with the analytical gel-filtration assay and MD simulations suggest that Cys163 of the helix plays a critical role in dimerization of the protein and thus for the stimulation of the activity.

As discussed earlier, this protein has a bimetallic center at the active-site, which is essential for the hydrolysis reaction. The metal binding assays showed that Trp159Phe, Trp159Ala and Asp126Ala exhibit loss of one metal. The disruption of the bimetallic center in these mutants is certainly one of the main reasons for complete loss of the catalytic activity. The MD simulations suggested a close contact (2.65 Å) between Trp159 and Asp126. Therefore, this interaction appears to be crucial in positioning the motif near the active-site, which is essential for the retention of the bimetallic center and function of the protein.

How do Trp159 and Asp126 play critical roles in retaining a bimetallic center at the active-site? Since the metal binding residues (first-shell residue) except Glu90 are primarily conserved in this protein (Figure S5, Supporting Information), Trp159 is unlikely to serve as a first-shell residue. However, in human arginase Trp122 has been found to act as a second-shell residue, which is strictly conserved in other arginases except *H. pylori*. This Trp forms a hydrogen bond through its indole moiety to the first-shell residue Asp124.[45] But *H. pylori* arginase shows a Tyr residue at this position. It has been suggested that in metalloproteins the geometry of the active-site appears to be shaped by second-shell residues for proper orientation of the inner residues to coordinate metal ions,[13,45] and the disruption of second-shell interactions can also result in loss of activity, which is observed in the case of argininemia patients.[13] Figure S5 (Supporting Information) showed a representation of the bimetallic center in *H. pylori* arginase based on the modeling and mutational studies, where $Co^{2+}{}_A$ is buried in the interior of the protein (analogous $Mn^{2+}{}_A$ is deeply localized in human arginase), whereas $Co^{2+}{}_B$ is relatively exposed (analogous $Mn^{2+}{}_B$ is exposed in human arginase).[19] We reported earlier that the conserved first-shell residues His91 and His118 are important in retaining one metal ion at the active-site. The mutational studies on these two histidine residues showed that the loss of metal ion in His118 metal binding site (corresponding metal is $Co^{2+}{}_B$, Figure S5) has a larger impact on the catalytic activity.[19] As observed in the MD simulations, Trp159 and Asp126 are close to the metal binding site (Figure 7A). It is possible that in the presence of the metal ions both Trp159 and Asp126 can move further closer to the metal binding site, as the MD simulations cannot be done in the presence of Co^{2+} ions owing to its limitation. On the basis of our biochemical data and metal analysis, it can be hypothesized that Trp159 may act as a second-shell residue to maintain the active-site architecture of the protein. Since Trp159 mutants individually displayed loss of one metal ion as well as complete loss of the catalytic activity, it is possible that Trp159 could interact with the first-shell residue His118 ($Co^{2+}{}_B$) through a salt bridge or directly via indole nitrogen. Similarly, Asp126 could act as a second-shell residue. It is interesting to note that the alignments of *H. pylori* arginase show Asp126 at the position of conserved Thr in mammalian and other bacterial arginases (Figure 2). The absence of the Trp122–Asp124 interaction (corresponding to human arginase) in *H. pylori* arginase might be complemented by the Trp159–Asp126 interaction. This also suggests that the active-site of *H. pylroi* arginase misses something critical compared to the homologous enzymes that is supplemented by the sequence motif.

Our data on Glu155Ala show that Glu155 is also crucial for the function, as its mutation results in complete loss of the activity although it has a bimetallic center. Hence, Glu155 appears to have a different role. The loss of activity in Glu155Ala is not due to the reduction in the secondary structure of the protein, as this mutant with 10% TFE restored the secondary structure but showed a marginal activity (2% of wild type). Thus, the loss of activity in Glu155Ala may be due to its inability to form a catalytically competent structure.

Arginase has been found to be a thermostable protein with $T_m \sim 70$ °C.[46] The higher T_m in arginases could be due to large numbers of secondary structural components, hydrophobic and/or electrostatic interactions. It is observed that mutations in the sequence motif severely compromise the thermostability of the apo-proteins. The decrease in the thermal stability of Trp159Ala and Glu155Ala compared to wild type in the absence of the metal ions is in agreement with the lower amount of the α-helical content, suggesting that hydrophobic and/or $\pi-\pi$, and electrostatic interactions by Trp159 and Glu155, respectively play crucial roles in maintaining the secondary structure of the whole protein. A close examination of Trp159 reveals that it makes hydrophobic and/or $\pi-\pi$ interactions with the surrounding aromatic amino acids Tyr125 and His122 (Figure 7D), indicating

that the loss of these interactions in Trp159Ala is likely to be the main reason for the decrease in the secondary structure and loss of stability. It was further supported by Trp159Phe, which resulted in an increase in the secondary structure and stability of the protein (Figure 9A).

Unlike wild type, the metal ions have also greater role in the stability to the mutants except Glu155Ala and Gln160Ala (Table 3), implying that the interactions of the metals with their ligands in the mutant proteins compensate the loss of stability. The T_m of Glu156Ala, Trp159Ala and Asp126Ala in the presence of the metal ions could not be determined reliably, as these mutants did not show proper heat-induced unfolding transitions, indicating that Glu156, Trp159 and Asp126 are also very crucial in maintaining the structure of the protein. Taken together, these results clearly demonstrate that the sequence motif is not only important for the stability of the protein, but also close to the active-site. It also demonstrates that in the absence of the metals the sequence motif plays a very vital role in providing electrostatic and hydrophobic interactions to maintain the overall structure of the protein.

In summary, we provide the evolutionary role of a non-conserved motif in *H. pylori* arginase, which is critical for multiple functions. The formation of an intact bimetallic cluster by Trp159 and Asp126 makes the protein catalytically competent as well significantly more stable to carry out the hydrolysis reaction of L-arginine for a continuous supply of polyamine precursor L-ornithine. The interaction of Trp159 with Asp126 appears to be crucial for bringing the motif close to the active-site so that the protein is stabilized by the hydrophobic and/or $\pi-\pi$ interactions of Trp159 with the surrounding aromatic amino acids. Glu155 provides a significant role in the structure and stability of the entire protein and is also important for catalysis. Simulation studies provide further insights into how the sequence motif is crucial for the structure and function of the protein. Furthermore, Cys163 of the small helix is primarily important for dimerization, which makes the protein catalytically more efficient for rapid depletion of L-arginine. This perhaps helps the bacterium to divert the substrate from the common competitive pool of iNOS in the host for the successful establishment of diseases caused by *H. pylori*. Hence, the motif can act as a regulatory switch. Our results thus provide the first report, where the sequence motif is not only critical for maintaining a catalytically competent conformation but also vital for the structure and stability of the whole protein. These findings imply that this stretch of the sequence motif can be engineered fully or partly in human arginase I and/or II to enhance their therapeutic potentials against a number of carcinomas such as hepatocellular, melanomas and prostate etc.,[47,48] as the engineered pegylated human arginase I and the chimeric enzymes of human arginase I and II[24] have been explicitly shown to provide long-term physiological stability and thus for better antineogenic agents against lymphoblastic T cell leukemia[22] and L-arginine auxotrophic tumors.[24] Our future challenge is also to extend in-depth understanding for mechanistic and biological investigations of *H. pylori* arginase, which may be important for therapeutics.

■ ASSOCIATED CONTENT

Supporting Information

Five figures of the structural analysis and a table of primers used in the study are provided. This material is available free of charge via the Internet at http://pubs.acs.org.

■ AUTHOR INFORMATION

Corresponding Author

*Tel: +91-11-26703768. Fax: +91-11-26742125/26742626. E-mail: apurbaksau@gmail.com; apurba@nii.res.in.

Author Contributions

#These authors contributed equally.

Notes

The authors declare no competing financial interest.

■ ACKNOWLEDGMENTS

This work was supported by the National Institute of Immunology and Indian Council of Medical Research, India. MD simulations were carried out on computing resources provided by the High Performance Computing Facility at the Inter University Accelerator Centre funded by the Department of Science and Technology, India.

■ ABBREVIATIONS

H. pylori, *Helicobacter pylori*; MD, Molecular dynamics simulation

■ REFERENCES

(1) Mendz, G. L., and Hazell, S. L. (1996) The urea cycle of *Helicobacter pylori*. *Microbiology 142* (Pt 10), 2959−2967.

(2) Sekowska, A., Danchin, A., and Risler, J. L. (2000) Phylogeny of related functions: the case of polyamine biosynthetic enzymes. *Microbiology 146* (Pt 8), 1815−1828.

(3) Tabor, H., and Tabor, C. W. (1972) Biosynthesis and metabolism of 1,4-diaminobutane, spermidine, spermine, and related amines. *Adv. Enzymol. Relat. Areas Mol. Biol. 36*, 203−268.

(4) Hovey, J. G., Watson, E. L., Langford, M. L., Hildebrandt, E., Bathala, S., Bolland, J. R., Spadafora, D., Mendz, G. L., and McGee, D. J. (2007) Genetic microheterogeneity and phenotypic variation of *Helicobacter pylori* arginase in clinical isolates. *BMC Microbiol. 7*, 26.

(5) McGee, D. J., Radcliff, F. J., Mendz, G. L., Ferrero, R. L., and Mobley, H. L. (1999) *Helicobacter pylori* rocF is required for arginase activity and acid protection in vitro but is not essential for colonization of mice or for urease activity. *J. Bacteriol. 181*, 7314−7322.

(6) Zabaleta, J., McGee, D. J., Zea, A. H., Hernandez, C. P., Rodriguez, P. C., Sierra, R. A., Correa, P., and Ochoa, A. C. (2004) *Helicobacter pylori* arginase inhibits T cell proliferation and reduces the expression of the TCR zeta-chain (CD3zeta). *J. Immunol. 173*, 586−593.

(7) Gobert, A. P., McGee, D. J., Akhtar, M., Mendz, G. L., Newton, J. C., Cheng, Y., Mobley, H. L., and Wilson, K. T. (2001) *Helicobacter pylori* arginase inhibits nitric oxide production by eukaryotic cells: a strategy for bacterial survival. *Proc. Natl. Acad. Sci. U. S. A. 98*, 13844−13849.

(8) Kanyo, Z. F., Chen, C. Y., Daghigh, F., Ash, D. E., and Christianson, D. W. (1992) Crystallization and oligomeric structure of rat liver arginase. *J. Mol. Biol. 224*, 1175−1177.

(9) Di Costanzo, L., Sabio, G., Mora, A., Rodriguez, P. C., Ochoa, A. C., Centeno, F., and Christianson, D. W. (2005) Crystal structure of human arginase I at 1.29-Å resolution and exploration of inhibition in the immune response. *Proc. Natl. Acad. Sci. U. S. A. 102*, 13058−13063.

(10) Kanyo, Z. F., Scolnick, L. R., Ash, D. E., and Christianson, D. W. (1996) Structure of a unique binuclear manganese cluster in arginase. *Nature 383*, 554−557.

(11) Cama, E., Colleluori, D. M., Emig, F. A., Shin, H., Kim, S. W., Kim, N. N., Traish, A. M., Ash, D. E., and Christianson, D. W. (2003) Human arginase II: crystal structure and physiological role in male and female sexual arousal. *Biochemistry 42*, 8445−8451.

(12) Garcia, D., Uribe, E., Lobos, M., Orellana, M. S., and Carvajal, N. (2009) Studies on the functional significance of a C-terminal S-shaped motif in human arginase type I: essentiality for cooperative effects. *Arch. Biochem. Biophys. 481*, 16−20.

(13) Bewley, M. C., Jeffrey, P. D., Patchett, M. L., Kanyo, Z. F., and Baker, E. N. (1999) Crystal structures of *Bacillus caldovelox* arginase in complex with substrate and inhibitors reveal new insights into activation, inhibition and catalysis in the arginase superfamily. *Structure 7*, 435−448.
(14) Muller, I. B., Walter, R. D., and Wrenger, C. (2005) Structural metal dependency of the arginase from the human malaria parasite *Plasmodium falciparum*. *Biol Chem 386*, 117−126.
(15) Carvajal, N., Acoria, M., Rodriguez, J. P., Fernandez, M., and Martinez, J. (1982) Evidence for cooperative effects in human liver arginase. *Biochim. Biophys. Acta 701*, 146−148.
(16) Christianson, D. W., and Cox, J. D. (1999) Catalysis by metal-activated hydroxide in zinc and manganese metalloenzymes. *Annu. Rev. Biochem. 68*, 33−57.
(17) Srivastava, A., and Sau, A. K. (2010) Biochemical studies on *Helicobacter pylori* arginase: insight into the difference in activity compared to other arginases. *IUBMB Life 62*, 906−915.
(18) McGee, D. J., Zabaleta, J., Viator, R. J., Testerman, T. L., Ochoa, A. C., and Mendz, G. L. (2004) Purification and characterization of *Helicobacter pylori* arginase, RocF: unique features among the arginase superfamily. *Eur. J. Biochem. 271*, 1952−1962.
(19) Srivastava, A., Dwivedi, N., Samanta, U., and Sau, A. K. (2011) Insight into the role of a unique SSEHA motif in the activity and stability of *Helicobacter pylori* arginase. *IUBMB Life 63*, 1027−1036.
(20) Azizian, H., Bahrami, H., Pasalar, P., and Amanlou, M. (2010) Molecular modeling of *Helicobacter pylori* arginase and the inhibitor coordination interactions. *J. Mol. Graph. Model. 28*, 626−635.
(21) Lee, G. K.-C., Kwok, S.-Y., Yu, C. H., Tam, K., Chong, H.-C., Leung, Y.-C., and Tsang, S. C. E. (2012) Immobilization of engineered arginase on gold-carbon nanotubes. *Chem. Commun. 48*, 7693−7695.
(22) Hernandez, C. P., Morrow, K., Lopez-Barcons, L. A., Zabaleta, J., Sierra, R., Velasco, C., Cole, J., and Rodriguez, P. C. (2010) Pegylated arginase I: a potential therapeutic approach in T-ALL. *Blood 115*, 5214−5221.
(23) Stone, E. M., Glazer, E. S., Chantranupong, L., Cherukuri, P., Breece, R. M., Tierney, D. L., Curley, S. A., Iverson, B. L., and Georgiou, G. (2010) Replacing Mn2+ with Co2+ in Human Arginase I Enhances Cytotoxicity toward l-Arginine Auxotrophic Cancer Cell Lines. *ACS Chem. Biol. 5*, 333−342.
(24) Romero, P. A., Stone, E., Lamb, C., Chantranupong, L., Krause, A., Miklos, A. E., Hughes, R. A., Fechtel, B., Ellington, A. D., Arnold, F. H., and Georgiou, G. (2012) SCHEMA-designed variants of human arginase I and II reveal sequence elements important to stability and catalysis. *ACS Synthetic Biol. 1*, 221−228.
(25) Tsui, S. M., Lam, W. M., Lam, T. L., Chong, H. C., So, P. K., Kwok, S. Y., Arnold, S., Cheng, P. N., Wheatley, D. N., Lo, W. H., and Leung, Y. C. (2009) Pegylated derivatives of recombinant human arginase (rhArg1) for sustained in vivo activity in cancer therapy: preparation, characterization and analysis of their pharmacodynamics in vivo and in vitro and action upon hepatocellular carcinoma cell (HCC). *Cancer Cell Int. 9*, 9.
(26) Lam, T. L., Wong, G. K., Chow, H. Y., Chong, H. C., Chow, T. L., Kwok, S. Y., Cheng, P. N., Wheatley, D. N., Lo, W. H., and Leung, Y. C. (2011) Recombinant human arginase inhibits the in vitro and in vivo proliferation of human melanoma by inducing cell cycle arrest and apoptosis. *Pigment Cell Melanoma Res. 24*, 366−376.
(27) Glazer, E. S., Stone, E. M., Zhu, C., Massey, K. L., Hamir, A. N., and Curley, S. A. (2011) Bioengineered human arginase I with enhanced activity and stability controls hepatocellular and pancreatic carcinoma xenografts. *Trans. Oncol. 4*, 138−146.
(28) Yau, T., Cheng, P. N., Chan, P., Chan, W., Chen, L., Yuen, J., Pang, R., Fan, S. T., and Poon, R. T. (2012) A phase 1 dose-escalating study of pegylated recombinant human arginase 1 (Peg-rhArg1) in patients with advanced hepatocellular carcinoma. *Invest New Drugs*, DOI: 10.1007/s10637-012-9807-9.
(29) Srivastava, A., Dwivedi, N., and Sau, A. K. (2010) Role of a disulphide bond in *Helicobacter pylori* arginase. *Biochem. Biophys. Res. Commun. 395*, 348−351.
(30) Purbey, P. K., Jayakumar, P. C., Patole, M. S., and Galande, S. (2006) pC6−2/caspase-6 system to purify glutathione-S-transferase-free recombinant fusion proteins expressed in *Escherichia coli*. *Nat. Protoc. 1*, 1820−1827.
(31) Iwig, J. S., Leitch, S., Herbst, R. W., Maroney, M. J., and Chivers, P. T. (2008) Ni(II) and Co(II) sensing by Escherichia coli RcnR. *J. Am. Chem. Soc. 130*, 7592−7606.
(32) Fan, H., and Mark, A. E. (2004) Refinement of homology-based protein structures by molecular dynamics simulation techniques. *Protein Sci. 13*, 211−220.
(33) Chen, J., Brooks, C. L., 3rd, and Khandogin, J. (2008) Recent advances in implicit solvent-based methods for biomolecular simulations. *Curr. Opin. Struct. Biol. 18*, 140−148.
(34) Ishitania, R., Teradaa, T., and Shimizu, K. (2008) Refinement of comparative models of protein structure by using multicanonical molecular dynamics simulations. *Mol. Simul. 34*, 327−336.
(35) Chopra, G., Summa, C. M., and Levitt, M. (2008) Solvent dramatically affects protein structure refinement. *Proc. Natl. Acad. Sci. U. S. A. 105*, 20239−20244.
(36) Lu, H., and Skolnick, J. (2003) Application of statistical potentials to protein structure refinement from low resolution ab initio models. *Biopolymers 70*, 575−584.
(37) Zhu, J., Fan, H., Periole, X., Honig, B., and Mark, A. E. (2008) Refining homology models by combining replica-exchange molecular dynamics and statistical potentials. *Proteins 72*, 1171−1188.
(38) Bernard, A. C., Mistry, S. K., Morris, S. M., Jr., O'Brien, W. E., Tsuei, B. J., Maley, M. E., Shirley, L. A., Kearney, P. A., Boulanger, B. R., and Ochoa, J. B. (2001) Alterations in arginine metabolic enzymes in trauma. *Shock 15*, 215−219.
(39) Kannan, S., and Zacharias, M. (2010) Application of biasing-potential replica-exchange simulations for loop modeling and refinement of proteins in explicit solvent. *Proteins 78*, 2809−2819.
(40) Louis-Jeune, C., Andrade-Navarro, M. A., and Perez-Iratxeta, C. (2012) Prediction of protein secondary structure from circular dichroism using theoretically derived spectra. *Proteins 80*, 374−381.
(41) Chen, Y. H., Yang, J. T., and Chau, K. H. (1974) Determination of the helix and beta form of proteins in aqueous solution by circular dichroism. *Biochemistry 13*, 3350−3359.
(42) McGaughey, G. B., Gagne, M., and Rappe, A. K. (1998) pi-Stacking interactions. Alive and well in proteins. *J. Biol. Chem. 273*, 15458−15463.
(43) Pandhare, J., Dash, C., Rao, M., and Deshpande, V. (2003) Slow tight binding inhibition of proteinase K by a proteinaceous inhibitor: conformational alterations responsible for conferring irreversibility to the enzyme-inhibitor complex. *J. Biol. Chem. 278*, 48735−48744.
(44) Ash, D. E. (2004) Structure and function of arginases. *J. Nutr. 134*, 2760S−2764S discussion 2765S-2767S.
(45) Stone, E. M., Chantranupong, L., and Georgiou, G. (2010) The second-shell metal ligands of human arginase affect coordination of the nucleophile and substrate. *Biochemistry 49*, 10582−10588.
(46) Scolnick, L. R., Kanyo, Z. F., Cavalli, R. C., Ash, D. E., and Christianson, D. W. (1997) Altering the binuclear manganese cluster of arginase diminishes thermostability and catalytic function. *Biochemistry 36*, 10558−10565.
(47) Feun, L. G., Marini, A., Landy, H., Markoe, A., Heros, D., Robles, C., Herrera, C., and Savaraj, N. (2007) Clinical trial of CPT-11 and VM-26/VP-16 for patients with recurrent malignant brain tumors. *J. Neurooncol. 82*, 177−181.
(48) Yoon, C. Y., Shim, Y. J., Kim, E. H., Lee, J. H., Won, N. H., Kim, J. H., Park, I. S., Yoon, D. K., and Min, B. H. (2007) Renal cell carcinoma does not express argininosuccinate synthetase and is highly sensitive to arginine deprivation via arginine deiminase. *Int. J. Cancer 120*, 897−905.